Photonic $\mathbb{Z}_2$ Topological Anderson Insulators

Xiaohan Cui, Ruo-Yang Zhang,* Zhao-Qing Zhang, and C. T. Chan†
Department of Physics, The Hong Kong University of Science and Technology, Hong Kong, China

(Received 10 February 2022; accepted 28 June 2022; published 19 July 2022)

That disorder can induce nontrivial topology is a surprising discovery in topological physics. As a typical example, Chern topological Anderson insulators (TAIs) have been realized in photonic systems, where the topological phases exist without symmetry protection. In this Letter, by taking transverse magnetic and transverse electric polarizations as pseudospin degrees of freedom, we theoretically propose a scheme to realize disorder-induced symmetry-protected topological phase transitions in two-dimensional photonic crystals with a combined time-reversal, mirror, and duality symmetry $\mathcal{T}_f = \mathcal{T}M_z\mathcal{D}$. In particular, we demonstrate that the disorder-induced symmetry-protected topological phase persists even without pseudospin conservation, thereby realizing a photonic $\mathbb{Z}_2$ TAI, in contrast to a $\mathbb{Z}$-classified quantum spin Hall (QSH) TAI with decoupled spins. By formulating a new scattering approach, we show that the topology of both the QSH and $\mathbb{Z}_2$ TAIs can be manifested by the accumulated spin rotations of the reflected waves from the photonic crystals. Using a transmission structure, we also illustrate the trivialization of a disordered QSH phase with an even integer topological index caused by spin coupling.

DOI: 10.1103/PhysRevLett.129.043902

Introduction.—As the photonic counterparts of the electronic topological insulators [1–7], topological photonic crystals (PCs) can support gapless edge states that are backscattering-immune against weak disorders [8–13]. However, if the disorders are sufficiently strong, the mobility band gap closes due to the Anderson localization, making the system topologically trivial [14–21]. Interestingly, recent studies report a reverse transition: disorders can drive PCs to change from a topologically trivial phase to a nontrivial phase. The systems in these disorder-induced topological phases are called topological Anderson insulators (TAIs) [22–35].

While the photonic TAI systems are mainly limited to Chern-type [31,32], the original discovery of TAIs stemmed from investigating disordered quantum spin Hall (QSH) systems with fermionic time-reversal (FTR) symmetry [22]. The initial idea of QSH effect is to build a system with two oppositely spin-polarized quantum Hall copies related by FTR symmetry [3,5]. However, Kane and Mele pointed out that even without s_z spin conservation, the FTR symmetry can protect nontrivial $\mathbb{Z}_2$ topological phase [4], which is different from the $\mathbb{Z}$ classified QSH phases with conserved spin current [36–38]. This surprising discovery gave rise to the notion of topological insulators and triggered the topological revolution in physics. In photonics, although QSH-like effects in ordered PCs had been widely studied in recent years [49–66], almost all these works are based on finding two decoupled pseudospin sectors, and the subtle but important difference between the QSH and $\mathbb{Z}_2$ topology had rarely been explored, aside from the discussion of a similar issue in the Floquet system [66]. Moreover, the study of disorder-induced TAI phase transition in QSH and $\mathbb{Z}_2$ systems also remains absent in photonics. The aim of this work is to fill these gaps.

In this Letter, we theoretically and computationally design a PC composed of pseudo-FTR symmetric media. By introducing geometric randomness, we observe the topological transitions from a trivial phase to QSH (with z-mirror symmetry) and $\mathbb{Z}_2$ (without z-mirror symmetry) TAI phases, which are demonstrated by the bulk transmission spectra and the helical edge states. To characterize the topology quantitatively, we connect the disordered PCs to a waveguide lead where we detect the pseudospin reflection from the PCs [67–78] and find that the windings of the reflected spins can characterize both the bulk $\mathbb{Z}$ and $\mathbb{Z}_2$ topological indices. In addition, we exhibit the difference between the QSH and $\mathbb{Z}_2$ TAI phases via boundary transport effects, which was rarely addressed in previous works.

$\mathcal{T}_f$-symmetric photonic crystals.—Surveying the literature of photonic QSH effects in 2D PCs, the underlying principle of nearly all schemes that are based on the special property of optical materials [51–63] can be traced to the hidden antiunitary symmetry $\mathcal{T}_f = \mathcal{T}M_z\mathcal{D}$, which combines time reversal $\mathcal{T}$, mirror reflection $M_z: (x, y, z) \to (x, y, -z)$, and electromagnetic duality transformation $\mathcal{D}: (\mathbf{E}, \mathbf{H}) \to (\mathbf{H}, -\mathbf{E})$ [60]. Since $\mathcal{T}_f^2 = -1$, $\mathcal{T}_f$ serves as a pseudo-FTR operator for photons. In the basis of the wave function $\Psi = (\mathbf{E}, \mathbf{H})^\intercal$, the operator takes the matrix representation $\mathcal{T}_f = -i\sigma_y \otimes m_z\mathcal{K}$, where σ_i $(i = x, y, z)$ denote the Pauli matrices, $m_z = \mathrm{diag}(1, 1, -1)$, and $\mathcal{K}$ denotes complex conjugate. The constitutive tensors of a $\mathcal{T}_f$-invariant photonic medium should respect $\overleftrightarrow{\varepsilon}/\varepsilon_0 = \begin{pmatrix} \overleftrightarrow{\varepsilon}_T & \boldsymbol{g} \\ \boldsymbol{g}^\dagger & \varepsilon_z \end{pmatrix}$, $\overleftrightarrow{\mu}/\mu_0 = \begin{pmatrix} \overleftrightarrow{\varepsilon}_T^* & -\boldsymbol{g}^* \\ -\boldsymbol{g}^\intercal & \varepsilon_z \end{pmatrix}$, where ε_0 and μ_0 are the

 © 2022 American Physical Society

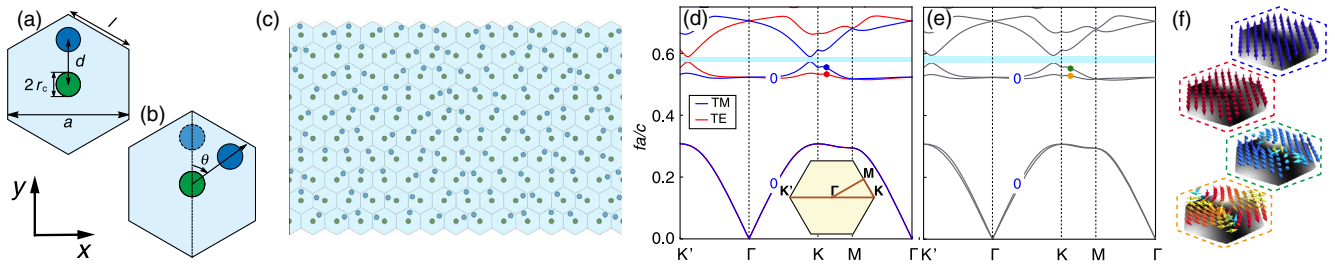

FIG. 1. (a) Unit cell of an ordered hexagonal PC with a lattice constant a. Parameters: $r_c = 0.1a$, $d = 0.37a$, $l = a/\sqrt{3}$. (b) One typical cell of the (c) disordered PC with the off-center cylinder rotated by a random angle θ. (d),(e) Band structures of two ordered PCs with (d) M_z symmetry ($\kappa = 0$) and without (e) M_z symmetry ($\kappa = 0.06$). (f) The distributions of pseudospins $\vec{s}$ (arrows) and intensity $\langle\psi|\psi\rangle$ (grayscale color map) of four eigenstates [labeled by the colored dots in (d) and (e)] with conserved and nonconserved pseudospins.

vacuum permittivity and permeability. Hereinafter, we let $\overleftrightarrow{\varepsilon}_T = \left(\begin{smallmatrix} 1 & i\beta \\ -i\beta & 1 \end{smallmatrix}\right)$ so that $\overleftrightarrow{\varepsilon}$ and $\overleftrightarrow{\mu}$ are gyrotropized in opposite manners [63], and we use $\boldsymbol{g} = (\kappa, \kappa)^\intercal$ to control the coupling between transverse electric (TE) and transverse magnetic (TM) modes. We stress that the use of gyrotropic media is only for computational convenience. Indeed, our theory is applicable to all $\mathcal{T}_f$-invariant systems, and the photonic $\mathbb{Z}_2$ TAIs can also be realized by reciprocal materials via a $SU(2)$ gauge transformation [38,79].

Figure 1(a) shows the unit cell of an ordered $\mathcal{T}_f$-invariant PC. The central gyrotropic cylinder (green) with $\beta = 0.7$, $\varepsilon_z = 25$, $\kappa = 0$ breaks the $\mathcal{T}$ symmetry, while the off-center reciprocal cylinder (blue) with $\beta = 0$, $\varepsilon_z = 5$, $\kappa = 0$ breaks the spatial inversion ($\mathcal{P}$) symmetry of the PC. If the background medium (light blue) has $\overleftrightarrow{\varepsilon}/\varepsilon_0 = \overleftrightarrow{\mu}/\mu_0 = 1$, $\kappa = 0$, the PC has M_z symmetry, and therefore the eigenstates can always be selected as TM (M_z odd) or TE (M_z even) polarized [see Fig. 1(d)]. In analogy to spin-1/2 fermions, we define the pseudospin of electromagnetic fields using the two-component spinor $|\psi\rangle = (E_z, \eta_0 H_z)^\intercal$ ($\eta_0 = \sqrt{\mu_0/\varepsilon_0}$ is the vacuum impedance) as

$$\vec{s} \equiv \langle\psi|\vec{\sigma}|\psi\rangle/\langle\psi|\psi\rangle, \tag{1}$$

with $\vec{\sigma} = \{\sigma_x, \sigma_y, \sigma_z\}$. Then, the TM and TE modes serve as pseudospin up and down states, respectively. The 2D Maxwell's equations with M_z symmetry are invariant under a $U(1)$ pseudospin rotation $U_s = \exp(i\vartheta\sigma_z/2)$ with an arbitrary angle ϑ [38], which guarantees the conservation of the s_z spin component [see Fig. 1(f)]. The symmetry-protected topological (SPT) phases with $\mathcal{T}_f$ and M_z symmetries are $\mathbb{Z}$ classified [36] by a QSH-Chern number C_s [38] [labeled on the bands in Fig. 1(d)]. The sum of C_s below the gap concerned (light blue) is 0, indicating the gap is topologically trivial. This is because the $\mathcal{P}$-breaking effect due to the off-center cylinder beats the $\mathcal{T}$-breaking effect induced by the central gyrotropic cylinder in each spin sector [38].

Next, we break M_z symmetry of the PC via adding the coupling term $\boldsymbol{g} = (\kappa, \kappa)^\intercal$ into the background medium. As shown in Fig. 1(e), the topologically trivial band gap remains open at $\kappa = 0.06$ [38], but the pseudospins of each Bloch mode are no longer uniformly polarized [see Fig. 1(f)]. Though the TM-TE coupling makes the QSH phases ill-defined [80], $\mathcal{T}_f$ symmetry itself can support a nontrivial SPT phase characterized by the Kane-Mele $\mathbb{Z}_2$ index ν [4], which is connected with the QSH-Chern number by $\nu = C_s \bmod 2$ in the weak coupling limit.

Disorder-induced topological phase transitions.—As shown in Figs. 1(b) and 1(c), we introduce disorders into the PCs with $\kappa = 0$ by rotating the off-center cylinder around the center one through a random angle θ (uniformly distributed in the interval $[-\theta_d/2, \theta_d/2]$) in each unit cell. In this way, we build disordered PC samples whose top and bottom boundaries are glued together continuously, and plane wave ports are imposed on the left and right boundaries. In the presence of M_z symmetry, one only need to consider the TM modes, since the TE modes correspond bijectively to the TM ones by $\mathcal{T}_f$ symmetry. We simulate the TM bulk transmission between the two ports over N random samples using COMSOL, and calculate the typical (geometric mean) transmittance $\langle T\rangle_{\text{typ}} = \exp[\sum_{n=1}^{N} \ln t_n/N]$ as a function of the disorder strength θ_d, as shown in Fig. 2(a), where t_n represents the TM transmittance of the nth sample. When disorder is weak, the transmission gap (dark region) corresponds to the topologically trivial band gap of the ordered PC in Fig. 1(d). As we increase θ_d, the mobility gap closes and reopens at around $\theta_d = 60°$, indicating the PC ensemble transitions into a QSH TAI phase, which can be verified by calculating the local QSH-Chern number [30,38,81]. The QSH TAI is nothing but two copies of Chern TAIs (TE and TM) related by $\mathcal{T}_f$ symmetry. Intuitively, the emergence of TAI phase in each spin sector occurs because strengthening the disorders can smooth out the $\mathcal{P}$ violations in different unit cells and makes the $\mathcal{T}$-breaking effect comparatively more dominant [38].

Turning now to the spin-coupled case ($\kappa = 0.06$), we let an obliquely polarized plane wave with $\mathbf{E} \propto (0, 1, 1)$ incident from the left port of the disordered PCs and collect

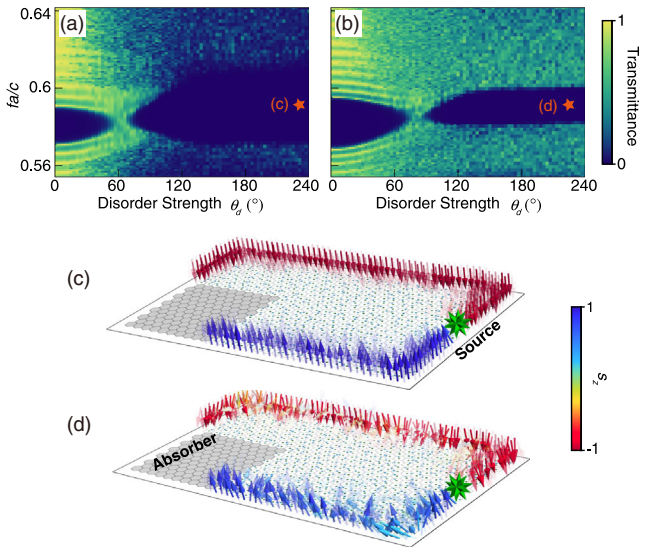

FIG. 2. Typical bulk transmittance averaged over $N = 10$ samples (size: $L_x \times L_y = 30a \times 30l$) for (a) spin-decoupled ($\kappa = 0$) and (b) coupled cases ($\kappa = 0.06$). (c),(d) Helical edge states in (c) a QSH TAI PC and in (d) a $\mathbb{Z}_2$ TAI PC [corresponding to the orange stars at $(\theta_d, f) = (220°, 0.59c/a)$ in (a),(b)]. Arrows' color and transparency represent the s_z component of pseudospins and the field intensity, respectively.

the total transmittance $\langle T\rangle_{\text{typ}} = \exp[\sum_{n=1}^{N} \ln(t_n + t'_n)/N]$ of both TE (t_n) and TM (t'_n) polarizations at the right port. The phase diagram in Fig. 2(b) also shows the process of mobility gap closing and reopening as the evidence of the disorder-induced transition from the trivial phase to the nontrivial $\mathbb{Z}_2$ TAI phase.

To demonstrate the two gapped phases after disorder-induced transitions indeed have nontrivial topology, we attempt to observe helical edge states on the boundaries of two disordered PCs in these phases with [Fig. 2(c)] and without [Fig. 2(d)] M_z symmetry [labeled by orange stars in Figs. 2(a) and 2(b)]. As shown in Figs. 2(c) and 2(d), a point source (green star) with superposed electric and magnetic monopoles is placed on the right boundary of each PC encased by a $\mathcal{T}_f$-symmetric insulation cladding with $\overleftrightarrow{\varepsilon}/\varepsilon_0 = \overleftrightarrow{\mu}/\mu_0 = \text{diag}(1, 1, -1)$. For the M_z-symmetric case [Fig. 2(c)], we observe that a purely spin-up surface wave (blue arrows) is emitted from the source and propagates clockwise along the boundaries, while a purely spin-down wave (red arrows) propagates counterclockwise along the boundaries due to $\mathcal{T}_f$ symmetry. This photonic QSH effect undoubtedly confirms the disorder-induced mobility gap is a TAI. In the case of breaking M_z symmetry, Fig. 2(d) shows that $\mathcal{T}_f$ symmetry can sustain the two counterpropagating surfaces waves; however, their spins are no longer uniformly polarized. Indeed, the whole disorder-induced phase permits bidirectional gapless boundary transportation, demonstrating that $\mathcal{T}_f$-invariant TAIs are compatible with spin coupling, which will be explained in Fig. 4(b).

Scattering approach for classifying disordered topological phases.—Inspired by the scattering approaches to retrieving the bulk topology [67–78], we propose a new spin-reflection method for calculating the topological invariants. As shown in Fig. 3(a), we connect a $\mathcal{T}_f$-symmetric dual-mode waveguide lead to the left end of the PC, and impose a twisted boundary condition with a twist angle ϕ_y to the two edges along the x direction of the PC [68,69] (see details and a possible experimental realization in the Supplemental Material (SM) [38]).

Considering the scattering process of an incident field $\psi_{\text{in}}(\phi_y, \omega)$ at frequency ω impinging upon the PC in the lead, the reflected spinor $\psi_{\text{r}}(\phi_y, \omega)$ is related to the incident spinor by a reflection matrix R: $\psi_{\text{r}}(\phi_y, \omega) = R(\phi_y, \omega)\psi_{\text{in}}(\phi_y, \omega)$. Within the mobility gap, $R(\phi_y, \omega)$ is a $U(2)$ matrix for the general PCs without M_z symmetry, and can be expressed as $R = e^{iq}\exp[i\alpha\vec{n}\cdot\vec{\sigma}]$ ($\vec{n}$ is a unit vector), whose eigenvalues $r_{1,2} = e^{i(q\pm\alpha)}$ represent two eigen reflection coefficients. Thanks to $\mathcal{T}_f$ symmetry, the reflection matrix satisfies [38]

$$\sigma_y R(\phi_y, \omega)^* \sigma_y = R(-\phi_y, \omega)^{\dagger}, \tag{2}$$

which gives rise to the Kramers' degeneracy of the two eigen reflection phases $\varphi_{1,2} = \arg(r_{1,2}) = q \pm \alpha$ at $\mathcal{T}_f$-invariant points ($\phi_0 = 0, \pi$), implying $R(\phi_0) = e^{iq}\sigma_0 \in U(1)$. As a consequence, the loops of the $\mathcal{T}_f$-symmetric reflection matrices over a cycle of ϕ_y are topologically classified by the relative homotopy group [38,82]

$$\pi_1(U(2), U(1)) = \pi_1(SO(3)) = \mathbb{Z}_2. \tag{3}$$

Akin to the Wilson loop approach [83], the two classes of $R(\phi_y)$ can be visually distinguished by the trivial and nontrivial connectivities of the concatenated trajectories of the two eigen reflection phases $\varphi_{1,2}$ in a half-period ($\phi_y \in [0, \pi]$) [see the two examples in Fig. 3(b)]. Choosing a smooth gauge of $\alpha(\phi_y)$, the $\mathbb{Z}_2$ index can also be calculated by the winding number of the relative phase $\Theta = \varphi_2 - \varphi_1 = -2\alpha$ over a half-period:

$$\tilde{\nu} = \left[\frac{1}{2\pi}\int_0^{\pi} d\phi_y \frac{\partial(\varphi_2 - \varphi_1)}{\partial\phi_y}\right] \mod 2 = 0 \text{ or } 1. \tag{4}$$

From the perspective of spin, after reflection from the disordered PC, the spin $\vec{s}_{\text{r}}$ of reflected wave rotates from the initial orientation $\vec{s}_{\text{in}}$ about the axis $\vec{n}$ by the angle $\Theta = -2\alpha$, as depicted in the inset of Fig. 3(a),

$$\vec{s}_{\text{r}} = G(\Theta, \vec{n})\vec{s}_{\text{in}} = \exp[\Theta\vec{n}\cdot\vec{\mathfrak{L}}]\vec{s}_{\text{in}}, \tag{5}$$

where $G(\Theta, \vec{n}) \in SO(3)$ is the spin-reflection matrix with $\vec{\mathfrak{L}}$ denoting the $\mathfrak{so}(3)$ generators. It is intriguing that the spin rotation angle is precisely the phase difference

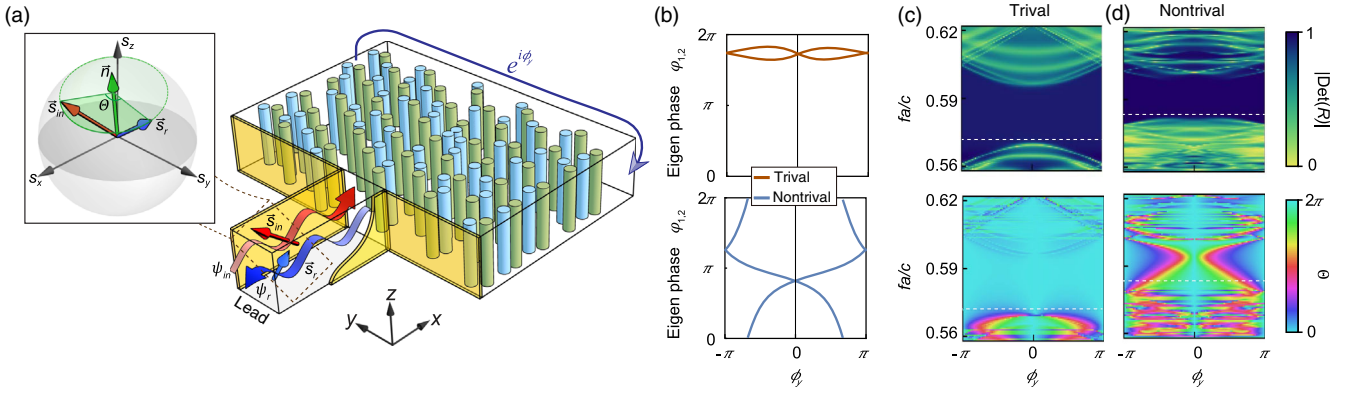

FIG. 3. (a) Schematic for retrieving the $\mathbb{Z}_2$ index from the spin reflection inside the waveguide lead connected to the disordered PC (size: $18a \times 15l$) with a twisted boundary condition $e^{i\phi_y}$. Inset (Bloch sphere): the rotation between the reflected and incident spins. (b) Eigen reflection phases in the trivial ($fa/c = 0.572$) and nontrivial ($fa/c = 0.583$) gaps. The total reflection magnitude $|\mathrm{Det}(R)|$ and the spin rotation angle Θ in the (c) trivial ($\theta_d = 20°$) and (d) nontrivial ($\theta_d = 220°$) gaps. The white dashed lines mark the frequencies of the eigen reflection phases in (b).

$\Theta = \varphi_2 - \varphi_1$ of the two eigen reflection coefficients. Therefore, although the rotation axis $\vec{n}(\phi_y)$ is generally unfixed caused by TM-TE coupling, the accumulated spin rotation angle $\Delta\Theta$ during a half cycle of ϕ_y remains quantized but can only take two stable values 0 and 2π, which reveals the physical meaning of the homotopy group $\pi_1(SO(3)) = \mathbb{Z}_2$ in Eq. (3) [38]. We also established the correspondence of the edge states and the relative phase and hence proved that the bulk topology is indeed equivalent to the $\mathbb{Z}_2$ classified accumulated spin rotation of the reflected waves [38].

Figures 3(c) and 3(d) plot $|\mathrm{Det}(R)|$ and the relative phase Θ for spin-coupled PCs ($\kappa = 0.06$) inside the trivial and TAI phases, respectively. By $\mathcal{T}_f$ symmetry, $\Theta(\phi_y)$ is symmetric about $\mathcal{T}_f$-invariant points at which it reduces to zero due to Kramers' degeneracy. Inside the mobility gaps ($|\mathrm{Det}(R)| = 1$) with weak [Fig. 3(c)] and strong [Fig. 3(d)] disorders, the winding numbers of $\Theta(\phi_y)$ over a half-period are fixed to 0 and 1, respectively. This result corroborates that the spin-coupled TAI phase in Fig. 2(b) possesses a well-defined $\mathbb{Z}_2$ topology.

For the PCs with M_z symmetry, due to the s_z spin conservation, the rotation axis $\vec{n}$ between the reflected and incident spins is fixed along s_z. As such, the spin rotation matrix reduces to $G = \exp[\Theta\mathfrak{L}_z] \in SO(2)$. Thus, after ϕ_y evolves over a half-period, the reflected spin will rotate about the s_z axis an integer number of times $C_s \in \pi_1(SO(2)) = \mathbb{Z}$, offering a spin rotation route to extracting the QSH-Chern numbers of the spin-decoupled TAI phases (see the numerical results in SM [38]). Note that our method does not require ensemble averaging, making it more efficient for computing topological indices of disordered systems than other approaches [84–86].

Distinction between QSH and $\mathbb{Z}_2$ TAIs.—According to the above discussions, the $\mathcal{T}_f$-symmetric PCs with and without M_z symmetry have different topological classifications, i.e., $\mathbb{Z}$ versus $\mathbb{Z}_2$. Now we examine this difference via edge transport effects.

We consider a strongly disordered PC whose bulk mobility gap shown in Fig. 4(a) is in the TAI phase with $C_s = 1$ at $\kappa = 0$. Turning on the spin coupling ($\kappa \neq 0$), the gap remains nontrivial with the $\mathbb{Z}_2$ index $\nu = 1$. The persistence of nontrivial topology is manifested by the gapless transmittance spectrum in Fig. 4(b), where the mobility gap (region between the two red dashed curves) is filled up by the gapless edge transport. For comparison, we build a domain wall between this PC ($\beta > 0$) and its time-reversal copy ($\beta < 0$) [see Fig. 4(c)]. At $\kappa = 0$, the two domains have opposite QSH-Chern numbers $C_s = \pm 1$. The nontrivial domain wall index $\Delta C_s = 2$ protects gapless interface transport at $\kappa = 0$. However, the emergence of spin coupling makes the two domains fall into the same $\mathbb{Z}_2$ class of $\nu = 1$, and immediately reduces the domain wall

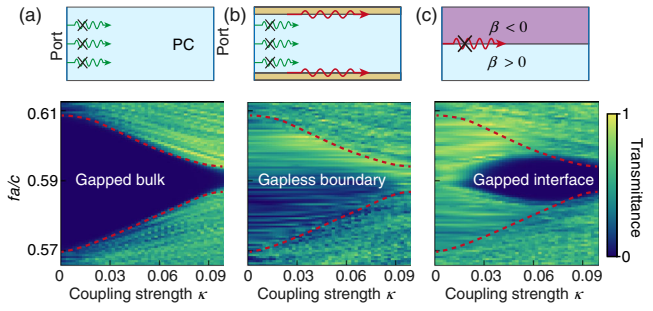

FIG. 4. Typical transmittance spectra (averaged over 15 samples) for the disordered PCs ($\theta_d = 150°$) with different transverse boundary conditions. (a) PC with continuously glued top and bottom boundaries. (b) PC sandwiched by $\mathcal{T}_f$-symmetric insulation cladding layers (orange). (c) Two PCs consisting of oppositely gyrotropized center cylinders ($\beta = \pm 0.7$, respectively) joined at two domain walls (center interface and top-bottom boundary). The red dashed curves denote the bulk mobility edges.

charge from $\Delta C_s = 2$ to $\Delta\nu = 0$. Consequently, the gapless transmission at $\kappa = 0$ opens a mobility gap as $\kappa \neq 0$, confirming that the domain wall topology is trivialized by the spin coupling.

Conclusion.—We proposed a scheme for realizing photonic QSH and $\mathbb{Z}_2$ TAIs supporting gapless helical edge transport in 2D disordered PCs with $\mathcal{T}M_z\mathcal{D}$ symmetry, where geometric disorder induces the transition from the trivial phase to the topological phases. Through observing the gapless to gapped transition of interface transport, we also verified that the absence or presence of the spin coupling changes the topological classification of the TAIs. Our system offers a prototypical platform to study photonic SPT phases with strong disorders. Furthermore, we developed a new approach to retrieve the QSH-Chern and $\mathbb{Z}_2$ indices of the disordered PCs from spin reflection, which is not only remarkably efficient for system without periodicity but also endows the topological invariants with the explicit physical meaning through the quantized spin rotation angles of the reflected waves during a half-period variation of the PCs' twisted boundaries. This approach is applicable to any systems with (pseudo)spins and would also be used to characterizing the $\mathbb{Z}_2$ charged 3D Dirac points [87–89].

We thank Professor Lei Zhang and Dr. Tianshu Jiang for helpful discussions. This work is supported by the Research Grants Council of Hong Kong (Grant No. 16307420).

*Corresponding author.
ruoyangzhang@ust.hk
†Corresponding author.
phchan@ust.hk

[1] M. Z. Hasan and C. L. Kane, Colloquium :Topological insulators, Rev. Mod. Phys. **82**, 3045 (2010).
[2] X.-L. Qi and S.-C. Zhang, Topological insulators and superconductors, Rev. Mod. Phys. **83**, 1057 (2011).
[3] C. L. Kane and E. J. Mele, Quantum Spin Hall Effect in Graphene, Phys. Rev. Lett. **95**, 226801 (2005).
[4] C. L. Kane and E. J. Mele, Z_2 Topological Order and the Quantum Spin Hall Effect, Phys. Rev. Lett. **95**, 146802 (2005).
[5] B. A. Bernevig and S.-C. Zhang, Quantum Spin Hall Effect, Phys. Rev. Lett. **96**, 106802 (2006).
[6] B. A. Bernevig, T. L. Hughes, and S.-C. Zhang, Quantum spin Hall effect and topological phase transition in HgTe quantum wells, Science **314**, 1757 (2006).
[7] D. N. Sheng, Z. Y. Weng, L. Sheng, and F. D. M. Haldane, Quantum Spin-Hall Effect and Topologically Invariant Chern Numbers, Phys. Rev. Lett. **97**, 036808 (2006).
[8] F. D. M. Haldane and S. Raghu, Possible Realization of Directional Optical Waveguides in Photonic Crystals with Broken Time-Reversal Symmetry, Phys. Rev. Lett. **100**, 013904 (2008).
[9] S. Raghu and F. D. M. Haldane, Analogs of quantum-Hall-effect edge states in photonic crystals, Phys. Rev. A **78**, 033834 (2008).
[10] Z. Wang, Y. D. Chong, J. D. Joannopoulos, and M. Soljačić, Reflection-Free One-Way Edge Modes in a Gyromagnetic Photonic Crystal, Phys. Rev. Lett. **100**, 013905 (2008).
[11] Z. Wang, Y. Chong, J. D. Joannopoulos, and M. Soljačić, Observation of unidirectional backscattering-immune topological electromagnetic states, Nature (London) **461**, 772 (2009).
[12] L. Lu, J. D. Joannopoulos, and M. Soljačić, Topological photonics, Nat. Photonics **8**, 821 (2014).
[13] T. Ozawa, H. M. Price, A. Amo, N. Goldman, M. Hafezi, L. Lu, M. C. Rechtsman, D. Schuster, J. Simon, O. Zilberberg, and I. Carusotto, Topological photonics, Rev. Mod. Phys. **91**, 015006 (2019).
[14] S. Mansha and Y. D. Chong, Robust edge states in amorphous gyromagnetic photonic lattices, Phys. Rev. B **96**, 121405(R) (2017).
[15] M. Xiao and S. Fan, Photonic Chern insulator through homogenization of an array of particles, Phys. Rev. B **96**, 100202(R) (2017).
[16] C. Liu, W. Gao, B. Yang, and S. Zhang, Disorder-Induced Topological State Transition in Photonic Metamaterials, Phys. Rev. Lett. **119**, 183901 (2017).
[17] P. Zhou, G.-G. Liu, X. Ren, Y. Yang, H. Xue, L. Bi, L. Deng, Y. Chong, and B. Zhang, Photonic amorphous topological insulator, Light Sci. Appl. **9**, 133 (2020).
[18] B. Yang, H. Zhang, Q. Shi, T. Wu, Y. Ma, Z. Lv, X. Xiao, R. Dong, X. Yan, and X. Zhang, Details of the topological state transition induced by gradually increased disorder in photonic Chern insulators, Opt. Express **28**, 31487 (2020).
[19] S. Yu, C.-W. Qiu, Y. Chong, S. Torquato, and N. Park, Engineered disorder in photonics, Nat. Rev. Mater. **6**, 226 (2021).
[20] B. Yang, H. Zhang, T. Wu, R. Dong, X. Yan, and X. Zhang, Topological states in amorphous magnetic photonic lattices, Phys. Rev. B **99**, 045307 (2019).
[21] P. Zhou, G.-G. Liu, X. Ren, Y. Yang, H. Xue, L. Bi, L. Deng, Y. Chong, and B. Zhang, Photonic amorphous topological insulator, Light Sci. Appl. **9**, 133 (2020).
[22] J. Li, R.-L. Chu, J. K. Jain, and S.-Q. Shen, Topological Anderson Insulator, Phys. Rev. Lett. **102**, 136806 (2009).
[23] C. W. Groth, M. Wimmer, A. R. Akhmerov, J. Tworzydło, and C. W. J. Beenakker, Theory of the Topological Anderson Insulator, Phys. Rev. Lett. **103**, 196805 (2009).
[24] Y. Xing, L. Zhang, and J. Wang, Topological Anderson insulator phenomena, Phys. Rev. B **84**, 035110 (2011).
[25] Y.-Y. Zhang, R.-L. Chu, F.-C. Zhang, and S.-Q. Shen, Localization and mobility gap in the topological Anderson insulator, Phys. Rev. B **85**, 035107 (2012).
[26] E. Prodan, Disordered topological insulators: A non-commutative geometry perspective, J. Phys. A **44**, 113001 (2011).
[27] P. Titum, N. H. Lindner, M. C. Rechtsman, and G. Refael, Disorder-Induced Floquet Topological Insulators, Phys. Rev. Lett. **114**, 056801 (2015).
[28] C. P. Orth, T. Sekera, C. Bruder, and T. L. Schmidt, The topological Anderson insulator phase in the Kane-Mele model, Sci. Rep. **6**, 24007 (2016).

[29] E. J. Meier, F. A. An, A. Dauphin, M. Maffei, P. Massignan, T. L. Hughes, and B. Gadway, Observation of the topological Anderson insulator in disordered atomic wires, Science **362**, 929 (2018).

[30] N. P. Mitchell, L. M. Nash, N. Hexner, T. A. M., and T. M. Irvine, Amorphous topological insulators constructed from random point sets, Nat. Phys. **14**, 380 (2018).

[31] S. Stützer, Y. Plotnik, Y. Lumer, P. Titum, N. H. Lindner, M. Segev, M. C. Rechtsman, and A. Szameit, Photonic topological Anderson insulators, Nature (London) **560**, 461 (2018).

[32] G.-G. Liu, Y. Yang, X. Ren, H. Xue, X. Lin, Y.-H. Hu, H.-x. Sun, B. Peng, P. Zhou, Y. Chong, and B. Zhang, Topological Anderson Insulator in Disordered Photonic Crystals, Phys. Rev. Lett. **125**, 133603 (2020).

[33] Z.-Q. Zhang, B.-L. Wu, J. Song, and H. Jiang, Topological Anderson insulator in electric circuits, Phys. Rev. B **100**, 184202 (2019).

[34] W. Zhang, D. Zou, Q. Pei, W. He, J. Bao, H. Sun, and X. Zhang, Experimental Observation of Higher-Order Topological Anderson Insulators, Phys. Rev. Lett. **126**, 146802 (2021).

[35] C. Wang, T. Cheng, Z. Liu, F. Liu, and H. Huang, Structural Amorphization-Induced Topological Order, Phys. Rev. Lett. **128**, 056401 (2022).

[36] K. Shiozaki and M. Sato, Topology of crystalline insulators and superconductors, Phys. Rev. B **90**, 165114 (2014).

[37] X.-G. Wen, Colloquium: Zoo of quantum-topological phases of matter, Rev. Mod. Phys. **89**, 041004 (2017).

[38] See Supplemental Material, which includes Refs. [39–48], at http://link.aps.org/supplemental/10.1103/PhysRevLett.129.043902 for (1) gauge transformation of $\mathcal{T}M_z\mathcal{D}$-symmetric materials, (2) the topology of ordered photonic crystals, (3) theoretical estimation of the TAI phase transition, (4) full-wave calculation of the local QSH-Chern number, (5) scattering approach for retrieving spin-Chern and $\mathbb{Z}_2$ indies, and (6) experimental proposal for mimicking the twisted boundary condition.

[39] X.-G. Wen, Quantum spin Hall state and $2+1$D topological insulator (2020), https://xgwen.mit.edu/blog/quantum-spin-hall-state-and-21d-topological-insulator.

[40] Y. Yang, Z. Xu, L. Sheng, B. Wang, D. Y. Xing, and D. N. Sheng, Time-Reversal-Symmetry-Broken Quantum Spin Hall Effect, Phys. Rev. Lett. **107**, 066602 (2011).

[41] E. Prodan, Robustness of the spin-Chern number, Phys. Rev. B **80**, 125327 (2009).

[42] L. Sheng, H.-C. Li, Y.-Y. Yang, D.-N. Sheng, and D.-Y. Xing, Spin Chern numbers and time-reversal-symmetry-broken quantum spin Hall effect, Chin. Phys. B **22**, 067201 (2013).

[43] Q.-X. Lv, Y.-X. Du, Z.-T. Liang, H.-Z. Liu, J.-H. Liang, L.-Q. Chen, L.-M. Zhou, S.-C. Zhang, D.-W. Zhang, B.-Q. Ai, H. Yan, and S. L. Zhu, Measurement of Spin Chern Numbers in Quantum Simulated Topological Insulators, Phys. Rev. Lett. **127**, 136802 (2021).

[44] K. Kawabata, K. Shiozaki, M. Ueda, and M. Sato, Symmetry and Topology in Non-Hermitian Physics, Phys. Rev. X **9**, 041015 (2019).

[45] M. Blanco de Paz, C. Devescovi, G. Giedke, J. J. Saenz, M. G. Vergniory, B. Bradlyn, D. Bercioux, and A. García-Etxarri, Tutorial: Computing topological invariants in 2D photonic crystals, Adv. Quantum Technol. **3**, 1900117 (2020).

[46] P. Sheng, *Introduction to Wave Scattering, Localization, and Mesoscopic Phenomena*, 2nd ed. (Springer, New York, 2006).

[47] R. B. Laughlin, Quantized Hall conductivity in two dimensions, Phys. Rev. B **23**, 5632 (1981).

[48] X.-Q. Sun, S.-C. Zhang, and T. Bzdušek, Conversion Rules for Weyl Points and Nodal Lines in Topological Media, Phys. Rev. Lett. **121**, 106402 (2018).

[49] M. Hafezi, E. A. Demler, M. D. Lukin, and J. M. Taylor, Robust optical delay lines with topological protection, Nat. Phys. **7**, 907 (2011).

[50] M. Hafezi, S. Mittal, J. Fan, A. Migdall, and J. M. Taylor, Imaging topological edge states in silicon photonics, Nat. Photonics **7**, 1001 (2013).

[51] A. B. Khanikaev, S. Hossein Mousavi, W.-K. Tse, M. Kargarian, A. H. MacDonald, and G. Shvets, Photonic topological insulators, Nat. Mater. **12**, 233 (2013).

[52] W.-J. Chen, S.-J. Jiang, X.-D. Chen, B. Zhu, L. Zhou, J.-W. Dong, and C. T. Chan, Experimental realization of photonic topological insulator in a uniaxial metacrystal waveguide, Nat. Commun. **5**, 5782 (2014).

[53] F. Liu and J. Li, Gauge Field Optics with Anisotropic Media, Phys. Rev. Lett. **114**, 103902 (2015).

[54] W.-J. Chen, Z.-Q. Zhang, J.-W. Dong, and C. T. Chan, Symmetry-protected transport in a pseudospin-polarized waveguide, Nat. Commun. **6**, 8183 (2015).

[55] T. Ma, A. B. Khanikaev, S. H. Mousavi, and G. Shvets, Guiding Electromagnetic Waves Around Sharp Corners: Topologically Protected Photonic Transport in Metawaveguides, Phys. Rev. Lett. **114**, 127401 (2015).

[56] T. Ochiai, Time-reversal-violating photonic topological insulators with helical edge states, J. Phys. Soc. Jpn. **84**, 054401 (2015).

[57] C. He, X.-C. Sun, X.-P. Liu, M.-H. Lu, Y. Chen, L. Feng, and Y.-F. Chen, Photonic topological insulator with broken time-reversal symmetry, Proc. Natl. Acad. Sci. U.S.A. **113**, 4924 (2016).

[58] X. Cheng, C. Jouvaud, X. Ni, S. H. Mousavi, A. Z. Genack, and A. B. Khanikaev, Robust reconfigurable electromagnetic pathways within a photonic topological insulator, Nat. Mater. **15**, 542 (2016).

[59] F. Gao, H. Xue, Z. Yang, K. Lai, Y. Yu, X. Lin, Y. Chong, G. Shvets, and B. Zhang, Topologically protected refraction of robust kink states in valley photonic crystals, Nat. Phys. **14**, 140 (2018).

[60] M. G. Silveirinha, PTD symmetry-protected scattering anomaly in optics, Phys. Rev. B **95**, 035153 (2017).

[61] S. Lannebère and M. G. Silveirinha, Photonic analogues of the Haldane and Kane-Mele models, Nanophotonics **8**, 1387 (2019).

[62] X. Ni, D. Purtseladze, D. A. Smirnova, A. Slobozhanyuk, A. Alù, and A. B. Khanikaev, Spin- and valley-polarized one-way Klein tunneling in photonic topological insulators, Sci. Adv. **4**, eaap8802 (2018).

[63] X.-C. Sun, C. He, X.-P. Liu, Y. Zou, M.-H. Lu, X. Hu, and Y.-F. Chen, Photonic topological states in a two-dimensional gyrotropic photonic crystal, Crystals **9**, 137 (2019).

[64] L.-H. Wu and X. Hu, Scheme for Achieving a Topological Photonic Crystal by Using Dielectric Material, Phys. Rev. Lett. **114**, 223901 (2015).
[65] S. Barik, H. Miyake, W. DeGottardi, E. Waks, and M. Hafezi, Two-dimensionally confined topological edge states in photonic crystals, New J. Phys. **18**, 113013 (2016).
[66] L. J. Maczewsky, B. Höckendorf, M. Kremer, T. Biesenthal, M. Heinrich, A. Alvermann, H. Fehske, and A. Szameit, Fermionic time-reversal symmetry in a photonic topological insulator, Nat. Mater. **19**, 855 (2020).
[67] D. Meidan, T. Micklitz, and P. W. Brouwer, Optimal topological spin pump, Phys. Rev. B **82**, 161303 (2010).
[68] D. Meidan, T. Micklitz, and P. W. Brouwer, Topological classification of adiabatic processes, Phys. Rev. B **84**, 195410 (2011).
[69] B. Sbierski and P. W. Brouwer, Z_2 phase diagram of three-dimensional disordered topological insulators via a scattering matrix approach, Phys. Rev. B **89**, 155311 (2014).
[70] I. C. Fulga, F. Hassler, and A. R. Akhmerov, Scattering theory of topological insulators and superconductors, Phys. Rev. B **85**, 165409 (2012).
[71] M. Xiao, Z. Q. Zhang, and C. T. Chan, Surface Impedance and Bulk Band Geometric Phases in One-Dimensional Systems, Phys. Rev. X **4**, 021017 (2014).
[72] W. S. Gao, M. Xiao, C. T. Chan, and W. Y. Tam, Determination of Zak phase by reflection phase in 1D photonic crystals, Opt. Lett. **40**, 5259 (2015).
[73] M. Pasek and Y. D. Chong, Network models of photonic Floquet topological insulators, Phys. Rev. B **89**, 075113 (2014).
[74] W. Hu, J. C. Pillay, K. Wu, M. Pasek, P. P. Shum, and Y. D. Chong, Measurement of a Topological Edge Invariant in a Microwave Network, Phys. Rev. X **5**, 011012 (2015).
[75] A. V. Poshakinskiy, A. N. Poddubny, and M. Hafezi, Phase spectroscopy of topological invariants in photonic crystals, Phys. Rev. A **91**, 043830 (2015).
[76] S. Mittal, S. Ganeshan, J. Fan, A. Vaezi, and M. Hafezi, Measurement of topological invariants in a 2D photonic system, Nat. Photonics **10**, 180 (2016).
[77] H. Wang, L. Zhou, and Y. D. Chong, Floquet Weyl phases in a three-dimensional network model, Phys. Rev. B **93**, 144114 (2016).
[78] H. Cheng, W. Gao, Y. Bi, W. Liu, Z. Li, Q. Guo, Y. Yang, O. You, J. Feng, H. Sun, J. Tian, S. Chen, and S. Zhang, Vortical Reflection and Spiraling Fermi Arcs with Weyl Metamaterials, Phys. Rev. Lett. **125**, 093904 (2020).
[79] Y. Chen, R.-Y. Zhang, Z. Xiong, Z. H. Hang, J. Li, J. Q. Shen, and C. T. Chan, Non-Abelian gauge field optics, Nat. Commun. **10**, 3125 (2019).
[80] L. Fu, Time reversal polarization and a Z_2 adiabatic spin pump, Phys. Rev. B **74**, 195312 (2006).
[81] A. Kitaev, Anyons in an exactly solved model and beyond, Ann. Phys. (Amsterdam) **321**, 2 (2006).
[82] A. Hatcher, *Algebraic Topology* (Cambridge University Press, Cambridge, England, 2002).
[83] R. Yu, X. L. Qi, A. Bernevig, Z. Fang, and X. Dai, Equivalent expression of Z_2 topological invariant for band insulators using the non-Abelian Berry connection, Phys. Rev. B **84**, 075119 (2011).
[84] T. A. Loring and M. B. Hastings, Disordered topological insulators via C^*-algebras, Europhys. Lett. **92**, 67004 (2010).
[85] H. Huang and F. Liu, Quantum Spin Hall Effect and Spin Bott Index in a Quasicrystal Lattice, Phys. Rev. Lett. **121**, 126401 (2018).
[86] Z. Li and R. S. K. Mong, Local formula for the Z_2 invariant of topological insulators, Phys. Rev. B **100**, 205101 (2019).
[87] B.-J. Yang and N. Nagaosa, Classification of stable three-dimensional Dirac semimetals with nontrivial topology, Nat. Commun. **5**, 4898 (2014).
[88] Q. Guo, B. Yang, L. Xia, W. Gao, H. Liu, J. Chen, Y. Xiang, and S. Zhang, Three Dimensional Photonic Dirac Points in Metamaterials, Phys. Rev. Lett. **119**, 213901 (2017).
[89] H. Cheng, Y. Sha, R. Liu, C. Fang, and L. Lu, Discovering Topological Surface States of Dirac Points, Phys. Rev. Lett. **124**, 104301 (2020).